International Journal of Heat and Mass Transfer 52 (2009) 1778–1785

Contents lists available at ScienceDirect

International Journal of Heat and Mass Transfer

journal homepage: www.elsevier.com/locate/ijhmt

Activated air plasma flow generated by pulsed arc discharge for combustion enhancement

H. Nishiyama *, K. Tsuri, H. Shimizu, K. Katagiri, H. Takana, Y. Nakano

Institute of Fluid Science, Tohoku University, 2-1-1, Katahira, Aoba-ku, Sendai 980-8577, Japan

ARTICLE INFO

Article history:
Received 1 June 2007
Received in revised form 10 October 2008
Available online 8 December 2008

Keywords:
Air plasma flow
Radicals
Pulsed arc discharge
Experiment
Modeling

ABSTRACT

Important operating parameters, temperature characteristics and radical production in an air plasma flow generated by a low-power pulsed arc discharge were experimentally clarified for lean combustion enhancement and surface treatment. Furthermore, the time-dependent thermofluid field downstream from the torch was also clarified numerically and the downstream temperature well agreed with experimental data. Finally, the time evolution of production and decay of the chemical species in air plasma were clarified numerically under a high electric field.

1. Introduction

Plasma flow has multifunctions of high energy density, chemical activation and electromagnetic controllability [1]. Thus, advanced technology for combustion enhancement in a scram jet [2–4], lean combustion in internal engine systems using activated plasma flow with radicals, plasma jet ignition [5,6] and surface treatment [7,8] have been intensively investigated. For example, it has been reported that soot formation is remarkably suppressed, flame propagation velocity is increased and ignition delay time is reduced by plasma assisted combustion [9]. This may result from an activated O radical, vibration excited molecules and NOx in air plasma [10,11]. Furthermore, plasma assisted combustion is expected to increase the fuel ratio and to extend the limit of lean combustion for clean exhaust gas when the intake air flow includes many activated radicals produced by pulsed discharge. Thus, it is very important to maximize production of oxygen radicals, metastable oxygen and nitrogen oxide molecules by pulsed discharge with minimized input power from the viewpoint of energy efficiency. As far as we know, there have been few papers on fundamental research on activated plasma flow including radicals for lean combustion enhancement and surface treatment.

In the present study, the effects of required input power, duty ratio, pulsed frequency and surrounding pressure on the temperature characteristics and concentrations of radicals in an air plasma flow by pulsed arc discharge were clarified experimentally. Moreover, a thermofluid field generated by pulsed arc discharge downstream of the torch was clarified numerically by introducing real operating conditions for comparison with experimental data on temperature. Finally, the time evolution of the production and decay processes of the various kinds of chemical species in an air plasma flow were clarified numerically for turning the high electric field on and off.

2. Experimental analysis

2.1. Experimental apparatus and measurement

Fig. 1 shows a schematic illustration of the experimental apparatus, which consists of a pulsed power supply (Hitachi Via Engineering Ltd., 350 CRL Model), on annular air plasma torch, an air supply system and a chamber. The anode is made of copper alloy and the cathode is made of tungsten alloy. The annular electrode gap in the plasma torch is 1 mm, and the applied pulsed voltage is about 4 kV. The range of duty ratio (discharge current time/period) is from 0.1 to 0.5 and that of pulsed frequency is from 100 to 1200 Hz for the power supply. The surrounding pressure in the chamber is changed from 20 to 120 kPa by a vacuum pump and a compressor.

The working gas is dried air, the flow rate into the torch being $1–9 \times 10^{-3}$ Nm^3/min. The gas temperature is measured by a copper-constantan thermocouple at 10, 15, 20 and 25 mm downstream from the torch exit. The radiation emitted from chemical species in an air plasma is measured at 15.7 mm downstream from the torch exit in the quartz tube by an instantaneous spectroscope (Ohtsuka Electric Co., MPCD-7000) ranging from 330 to 1100 nm.

* Corresponding author. Tel./fax: +81 22 217 5260.
E-mail address: nishiyama@ifs.tohoku.ac.jp (H. Nishiyama).

0017-9310/$ - see front matter © 2008 Elsevier Ltd. All rights reserved.
doi:10.1016/j.ijheatmasstransfer.2008.10.009

Nomenclature

e	stagnant internal energy (J/m^3)	T_e	electron temperature (K)
E	electric field strength (V/m)	u	axial velocity (m/s)
f	pulsed frequency (Hz)	V	applied voltage (V)
I	discharge current (A)	v	radial velocity (m/s)
N	number density ((m^3)$^{-1}$)	z	axial coordinate (m)
P_{in}	input electric power (W)		
P_0	surrounding pressure (Pa)	*Greek*	
Q	gas flow rate (m^3/min)	η	heat input efficiency
Q_{arc}	thermal generation by pulsed arc (W/m^3)	λ	thermal conductivity (W/(m K))
Q_{rad}	radiation loss (W/m^3)	ρ	density (kg/m^3)
r	radial coordinate (m)	τ	shear stress (Pa)
R	gas constant (J/(kg K))	Φ_D	viscous dissipation (W/m^3)
t	time (s)	θ	azimuthal coordinate (rad)
T	gas temperature (K)		

The produced O, NO, O_2 and N_2 in the air flow are measured by a mass spectrometer (ANELVA Co., M-200GA-DM) through a glass tube 0.075 mm in diameter and 1.5 mm length introduced from the chamber to show only the relative small variations of radical species.

2.2. Experimental results and discussion

Fig. 2 shows the applied voltage and discharge current at a pulsed frequency of 100 Hz, a duty ratio of 0.2 and surrounding pressure of 100 kPa. An applied pulsed high voltage of 4 kV with microsecond rise starts the breakdown of the air flow at 10^{-3} Nm^3/min, following a sustainable current discharge flow. After the input electric energy is consumed, the discharge current flow disappears automatically. Here, the duty ratio is defined as the continuous discharge current time for a pulse period. This shows that the time-averaged input power is about 300 W, which requires smaller energy to generate a pulsed arc compared with a continuous DC arc.

Fig. 3(a) and (b) show side and bottom views of the air plasma flow at a pulsed frequency of 600 Hz, a duty ratio of 0.2 and a surrounding pressure of 100 kPa. When the inlet air flow rate increases, air plasma first elongates due to increasing axial velocity, but then becomes sharp at a flow rate of 9×10^{-3} Nm^3/min due to the decrease in the net effective input enthalpy to the air flow. Furthermore, the arc spot rotates azimuthally around the annular electrodes.

Fig. 4(a) and (b) show the downstream gas temperatures at the centerline with the duty ratio and pulsed frequency, respectively. The downstream gas temperature increases with an increase in the duty ratio due to the increasing effective input electrical power. The maximum temperature nearest the torch exit ($T1$) is 700 K at a duty ratio of 0.5, but the minimum temperature ($T4$) farthest downstream is 350 K. The increasing rate of gas temperature increases remarkably with a large duty ratio near the torch exit ($T1$). On the other hand, the gas temperature does not greatly change for pulsed frequency at any of the measurement points due to the constant duty ratio.

Fig. 5 shows the power spectrum of radiative species in an air plasma flow at a pulsed frequency of 600 Hz, a duty ratio of 0.2 and surrounding pressure of 100 kPa. The required electric power is 226 W and the air flow rate is 3×10^{-3} Nm^3/min. The emissive oxygen atom OI (777.3, 822.2, 844.6, 926.0 nm) and nitrogen atom NI (746.8, 818.8, 868.3 nm) can be observed even for small input electric power [12]. However, a strong emission from the copper and tungsten electrode materials is also observed at a small wave

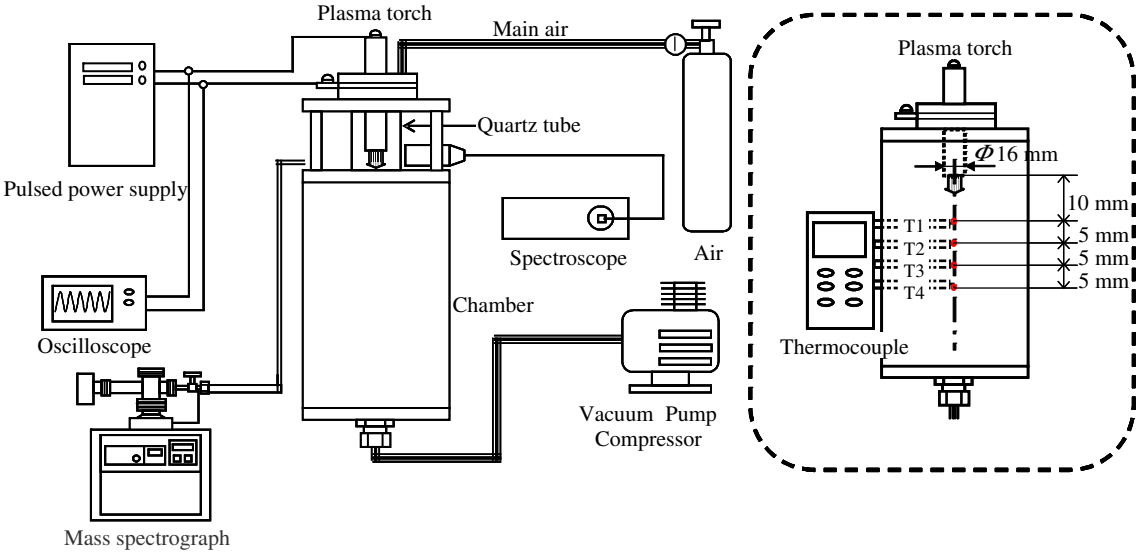

Fig. 1. Schematic illustration of experimental apparatus.

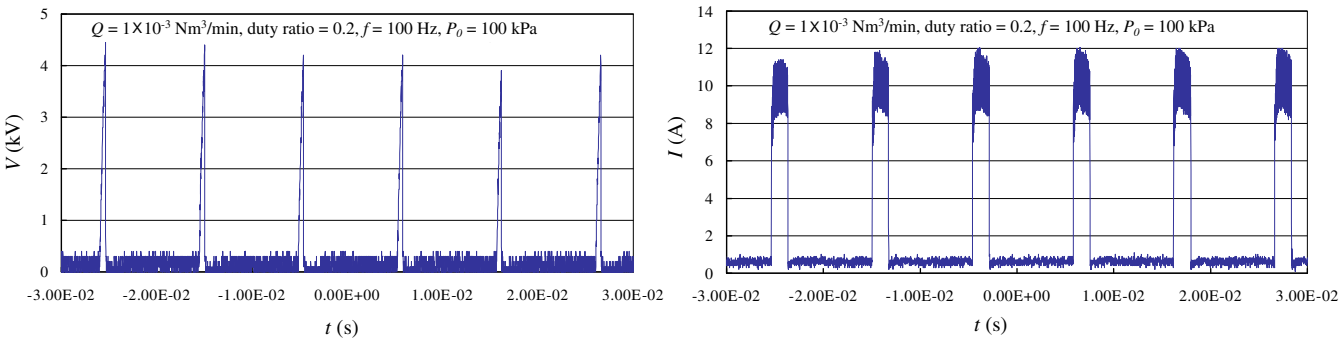

Fig. 2. Applied voltage and discharge current.

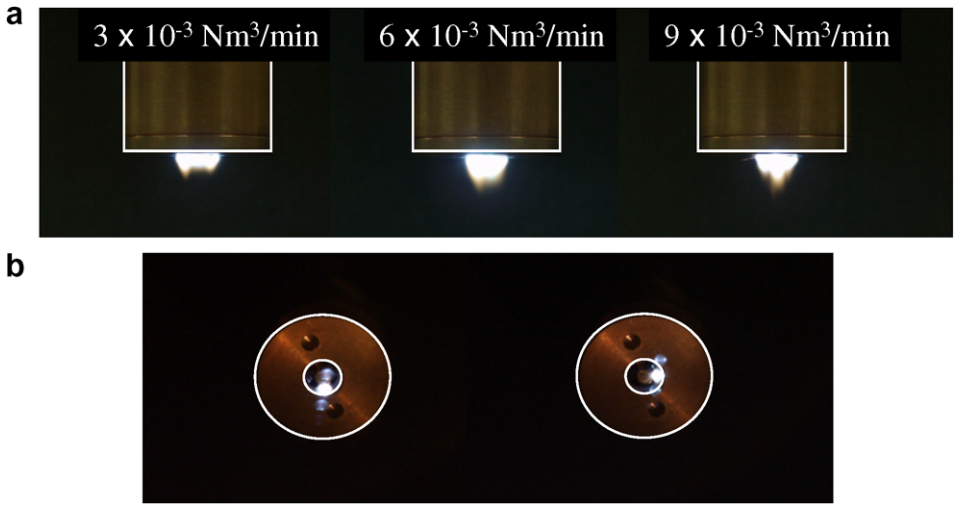

Fig. 3. Photo of air plasma flow.

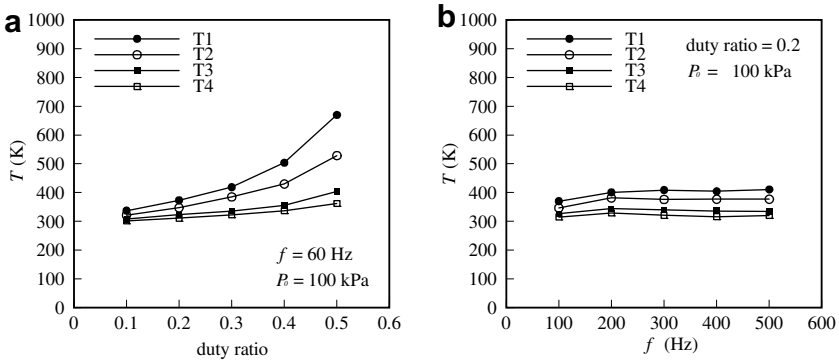

Fig. 4. Downstream gas temperature (a) with duty ratio (b) with pulsed frequency.

length due to the sputter. Thus, weak radiation from molecular nitrogen such as a second positive band cannot be detected by our spectrometer at the same wave band.

Fig. 6 shows the radiative intensity from an oxygen atom (777.3 nm) with duty ratios for all surrounding pressures. The radiative intensity corresponds to the produced number density of the oxygen radical, which is useful for combustion enhancement, surface oxidation and nitrization. The radiative intensity increases with an increase in the duty ratio for higher surrounding pressure. This tendency is nearly the same as that of the gas temperature as shown in Fig. 4. This means that the produced oxygen radicals increase remarkably, especially for larger duty ratios at high surrounding pressure even less than 380 W.

Fig. 7 shows the relative variation of chemical species 5 mm downstream from the torch exit with and without discharge measured by a mass spectrometer, the large amount of N_2 being neglected in order to emphasize the small variation of O_2 and NO in this scale. In the case of discharge, O_2 slightly decreases due to decomposition and NO is observed as a second product after recombination. However, O and N are not clearly detected for longer sampling time of air plasma in the present experimental method due to their short lifetime. Then, O and N with short lifetimes are

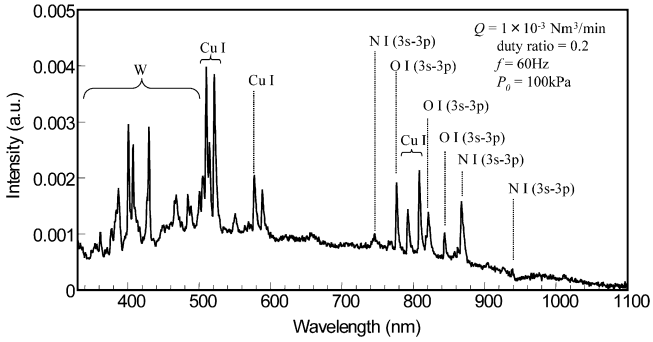

Fig. 5. Power spectrum from radiative species.

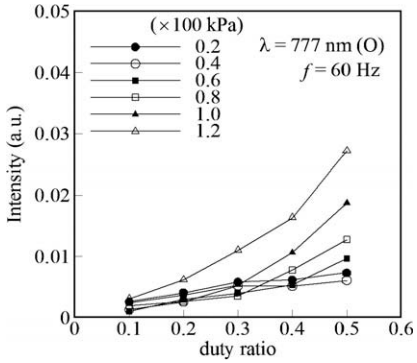

Fig. 6. Radiative intensity from the O atom (777.3 nm) with duty ratio.

transferred to NO for a short time as the following chemical reactions.

$$\begin{cases} e + O_2 \rightarrow e + O + O \\ e + N_2 \rightarrow e + N + N \\ O + N_2 \rightarrow N + NO \\ N + O_2 \rightarrow O + NO \\ N + O + M \rightarrow NO + M \end{cases}$$

3. Numerical analysis of thermofluid field

3.1. Governing equations

Fig. 8 shows a schematic illustration of the numerical model. To derive the governing equations for thermofluid fields in a torch and downstream of the torch, the following assumptions are introduced here.

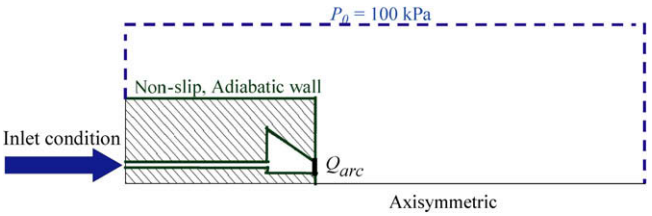

Fig. 8. Schematic illustration of numerical model.

(1) Plasma is regarded as a continuous and compressible flow in local thermodynamic equilibrium.
(2) The thermofluid field is turbulent [13] and axisymmetrical 2D.
(3) Air has temperature dependent thermodynamic and transport properties [14].
(4) Initial composition of air as a working gas is N_2:O_2 = 4:1 before discharge.
(5) Thermal input by a pulsed arc is given as Q_{arc} in the equation of energy without solving the electromagnetic field.

The governing equations for the thermofluid field are as follows:

Equation of continuity

$$\frac{\partial \rho}{\partial t} + \frac{\partial}{\partial z}(\rho u) + \frac{1}{r}\frac{\partial}{\partial r}(r\rho v) = 0 \tag{1}$$

Equation of momentum

$$\frac{\partial}{\partial t}(\rho u) + \frac{\partial}{\partial z}(\rho u^2) + \frac{1}{r}\frac{\partial}{\partial r}(r\rho u v) = -\frac{\partial p}{\partial z} + \frac{\partial}{\partial z}\tau_{zz} + \frac{1}{r}\frac{\partial}{\partial r}(r\tau_{rz}) \tag{2}$$

$$\frac{\partial}{\partial t}(\rho v) + \frac{\partial}{\partial z}(\rho u v) + \frac{1}{r}\frac{\partial}{\partial r}(r\rho v^2) = -\frac{\partial p}{\partial r} + \frac{\partial}{\partial z}\tau_{rz} + \frac{1}{r}\frac{\partial}{\partial r}(r\tau_{rr}) - \frac{\tau_{\theta\theta}}{r} \tag{3}$$

Equation of energy

$$\frac{\partial e}{\partial t} + \frac{\partial}{\partial z}\{(e+p)u\} + \frac{1}{r}\frac{\partial}{\partial r}\{r(e+p)v\} = \frac{\partial}{\partial z}\left(\lambda\frac{\partial T}{\partial z}\right) + \frac{1}{r}\frac{\partial}{\partial r}\left\{r\left(\lambda\frac{\partial T}{\partial r}\right)\right\} + \Phi_D - Q_{rad} + Q_{arc} \tag{4}$$

Equation of state

$$p = \rho RT \tag{5}$$

3.2. Boundary conditions and initial condition

The boundary conditions and heat input condition for determining the flow and temperature fields are described here. Heat input:

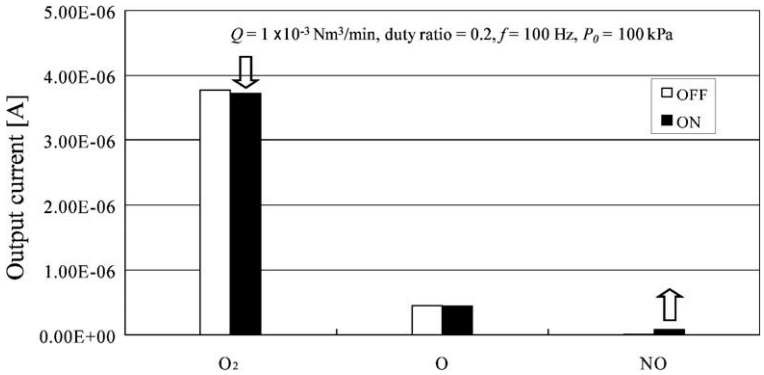

Fig. 7. Relative amount of chemical species with discharge on and off.

$P_{in} = 500\ \mathrm{W}, \quad f = 500\ \mathrm{Hz}, \quad \text{duty ratio} = 0.2, \quad \eta = 0.5,$

$Q_{arc} = \eta P_{in}$

Torch inlet:

$$u = 3\ \mathrm{m/s}, \quad v = 0\ \mathrm{m/s}, \quad T = 300\ \mathrm{K}, \quad \frac{\partial p}{\partial n} = 0$$

Torch inner and outer wall:

$$u = v = 0\ \mathrm{m/s}, \quad T = 300\ \mathrm{K}, \quad \frac{\partial p}{\partial n} = 0$$

Free boundary:

$$\frac{\partial u}{\partial n} = \frac{\partial v}{\partial n} = 0, \quad \frac{\partial \rho}{\partial n} = 0, \quad p_0 = 100\ \mathrm{kPa}$$

Axis:

$$\frac{\partial u}{\partial r} = 0, \quad v = 0\ \mathrm{m/s}, \quad \frac{\partial P}{\partial r} = \frac{\partial \rho}{\partial r} = 0$$

The initial conditions are given as $u = v = 0$ m/s, $T = 300$ K and $p = 100$ kPa. Discharge is started after obtaining a steady flow field in the torch. Heat input efficiency η is assumed to be 0.5 at most to generate the arc referring to the conventional case.

The LU-SGS method coupled with the Newtonian interactive method is used for time integration, and the Roe flux differential method coupled with the 3rd-order MUSCL-type TVD scheme is used for the convective term, respectively. The Smagorinsky model in Large Eddy Simulation (LES) is adopted for compressible turbulent flows [13].

3.3. Numerical results and discussion

Fig. 9 shows the time evolution of the axial velocity at every 1 ms during eight pulsations. A pulsed discharge occurs at every 2 ms, the discharge duration being 0.4 ms for a duty ratio of 0.2. A jet is issued about 90 m/s from the torch exit due to thermal expansion. The jet continuously elongates downstream at 40 m/s at each discharge.

Fig. 10 shows the time evolution of gas temperature at every 1 ms. A thermal vortex with a temperature of 4500 K is generated at the torch exit at every pulsed discharge and is diffused downstream. The diameter of the thermal vortex is about 1 mm and its core temperature is about 3000 K at the end of the discharge. Its downstream convective velocity of interaction with other vortices is small. At about 6 ms after discharge, the vortex temperature decreases about 1000 K due to turbulent diffusion. The temperatures at $T1$, $T2$, $T3$ and $T4$ range from 1000 to 1500 K intermittently, corresponding to a pulsed discharge about 8 ms after discharge.

Fig. 11 shows a comparison of the numerically time-averaged temperature at the centerline with the experimental data, which corresponds to a bulk mean temperature. Time averaging is

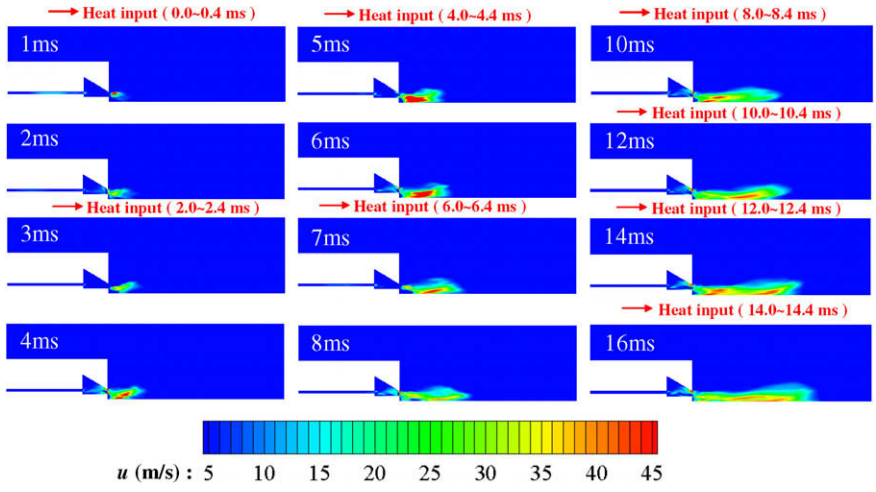

Fig. 9. Time evolution of axial velocity.

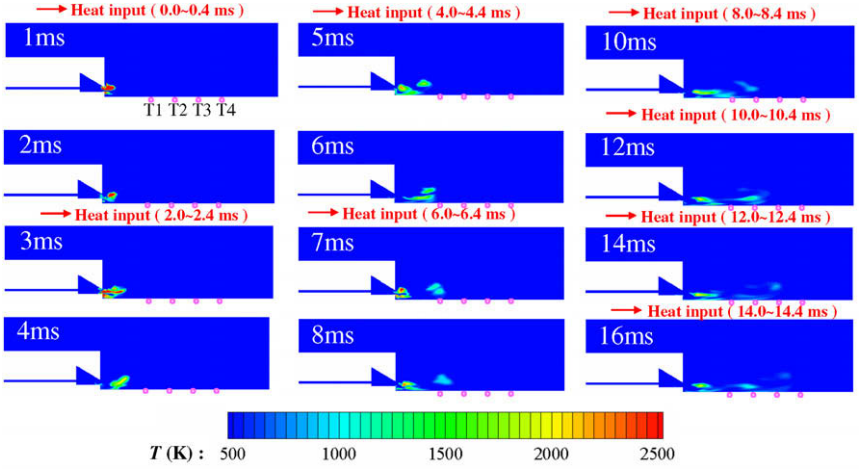

Fig. 10. Time evolution of gas temperature.

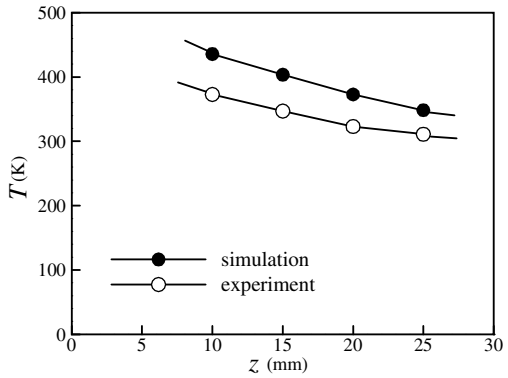

Fig. 11. Comparison of centerline gas temperature with experimental data.

conducted from 8 to 20 ms for unsteady temperature, which depends on heat input only during discharge. The tendency of the downstream temperature shows good agreement with the experimental data within a 50 K difference depending on the time-averaging period.

4. Radical production and decay processes

4.1. Assumptions

The electron impact process by application of high voltage is the dominant chemical reaction which produces various kinds of activated radicals in the air [15]. Kossyi proposed about 300 chemical reaction equations for non-equilibrium air plasma [15–17]. However, it is important to reduce the number of equations for complex chemical reactions to reduce computational time.

Thus, the simplified reaction model by Benilov [18] is applied to clarify the radical production processes in a discharge region. The following assumptions are introduced here.

(1) Flow effect is neglected compared with rapid chemical reactions in a discharge region.
(2) Applied electric field and concentration field are spatially uniform.
(3) Electron impact reactions have spatial uniformity.
(4) Electron temperature is as a function of E/N, which is the ratio of the electric field to the number density of air in a non-equilibrium state.
(5) Initial composition of air is N_2:O_2 = 4:1 before discharge.
(6) It is assumed that $10^9/m^3$ electrons exist by the cosmic ray [19].

4.2. Constituent conservation equation

The constituent conservation equation, neglecting diffusion, is as follows:

$$\left.\begin{aligned} \frac{dN_i}{dt} &= S_i^+ - S_i^- \\ N_e &= N^+ - N^- \end{aligned}\right\}, \tag{6}$$

where N_i is the number density of i species, and S_i^+ and S_i^- are production rate and recombination rate per unit time, respectively. The number of chemical species considered was 15 in the present study. Table 1 shows 30 chemical reactions and rate constants for simpli-

Table 1
Chemical reactions and rate constants.

List of reactions			
Number	Reaction	Rate constant	Ref.
1	$e + N_2 \rightarrow e + e + N_2^+$	8.1×10^{-15}exp[-925/(E/N)]F	a
2	$e + O_2 \rightarrow e + e + O_2^+$	4.9×10^{-15}exp[-657/(E/N)]F	a
3	$e + NO \rightarrow e + e + NO^+$	5.0×10^{-15}exp[-460/(E/N)]F	a
4	$e + O \rightarrow e + e + O^+$	4.0×10^{-15}exp[-713/(E/N)]F	a
5	$e + N_2 \rightarrow e + N + N$	2.0×10^{-11}	e
6	$e + O_2 \rightarrow e + O + O$	exp[−7.9−134/(E/N)] + exp[−8.0−169/(E/N)] + exp[−8.8−119/(E/N)]	b
7	$N + O \rightarrow NO^+ + e$	1.0×10^{-12}	b
8	$NO^+ + e \rightarrow N + O$	$1.1 \times 10^{-2} T_e^{-1.5}$	c
9	$N_2 + M \rightarrow N + N + M$	$[5.5 \times 10^{-14}(X_{N2} + X_{O2} + X_{NO})][1 - \exp(-E_{N2}/T)]\exp(-D_{N2}/T)$	a
10	$N + N + M \rightarrow N_2 + M$	$8.27 \times 10^{-27}\exp(500/T)$	b
11	$O_2 + M \rightarrow O + O + M$	$[9.1 \times 10^{-15}(X_{N2} + X_{O2} + X_{NO}) + 3.6 \times 10^{-14}X_{O2} + 1.3 \times 10^{-13}X_o]1 - \exp(-E_{O2}/T)]\exp\{-D_{O2}/T)$	a
12	$O + O + M \rightarrow O_2 + M$	$2.76 \times 10^{-34}\exp(720/T)$	b
13	$NO + M \rightarrow N + O + M$	$[1.0 \times 10^{-14}(X_{N2} + X_{O2}) + 2.0 \times 10^{-13}(X_{NO} + X_O + X_{NO})][1 - \exp(-E_{NO}/T)]\exp(-D_{NO}/T)$	a
14	$N + O + M \rightarrow NO + M$	K_{13}/B_{NO}	a
15	$N + NO \rightarrow O + N_2$	3.0×10^{-11}	d
16	$O + N_2 \rightarrow N + NO$	$K_{15}/B_{N2}/B_{NO}$	a
17	$N + O_2 \rightarrow O + NO$	$4.5 \times 10^{-12}(-3220/T)$	b
18	$O + NO \rightarrow N + O_2$	4.0×10^{-11}	d
19	$e + O_2 + O_2 \rightarrow O_2^- + O_2$	$3.6 \times 10^{-43} T_e^{-1}\exp(-0.052/T)\exp[0.06(T_e - T)/T_e/T]$	a
20	$e + O_2 \rightarrow O^- + O$	6.7×10^{-19}exp(−1.05|5.3−h(E/N)0.8)F	a
21	$O_2^- + O_2 \rightarrow e + O_2 + O_2$	$2.0 \times 10^{-16}\exp(-3220/T)$ [1−exp(−4θ)]/[1−exp(−θ)	a
22	$O^- + N_2 \rightarrow N_2O + e$	9.0×10^{-19}	a
23	$O^- + O \rightarrow O_2 + e$	5.0×10^{-16}	a
24	$O^- + NO \rightarrow NO_2 + e$	2.6×10^{-19}	a
25	$O_2^- + O \rightarrow O_3 + e$	1.5×10^{-19}	a
26	$O_3^- \rightarrow O_2 + O_2 + e$	3.0×10^{-19}	a
27	$O^- + O_2 + M \rightarrow O_3^- + M$	$2.8 \times 10^{-44} T_{ef1}^{-1}$	a
28	$X^- + Y^+ \rightarrow X + Y$	$2.0 \times 10^{-7}(300/T_{ion})^{0.5}$	b
29	$e + O_2^+ \rightarrow O + O$	$2.0 \times 10^{-7}(300/T_e)^{0.7}$	b
30	$e + N_2^+ \rightarrow N + N$	$2.8 \times 10^{-7}(300.T_e)^{0.7}$	b

a: M.S. Benilov, G.V. Naidis, J. Phys. D: Appl. Phys., 36, (2003) pp. 1834–1841.
b: I.A. Kossiy, Plasma Sources Sci. Technol., 1, (1992) pp. 207.
c: N.L. Aleksandrov, J. Phys. D: Appl. Phys., 30, (1997) pp. 1616–1624.
d: J.T. Herron, Plasma chemistry and plasma processing, 21, 4, (2001) pp. 459–481.
e: M. Castillo, et al., Plasma sources, Sci. Technol., 13, (2004) pp. 343–350.

fication. The rate constants are given as functions of electron temperature and gas temperature. The electron temperature is given by E/N as follows [15]:

$$T_e = 0.447\left(\frac{E}{N}\right)^{0.36} \quad : \frac{E}{N} < 50$$
$$T_e = 0.0167\frac{E}{N} \quad : \frac{E}{N} > 50 \tag{7}$$

4.3. Numerical results and discussion

Fig. 12 shows the time evolution of the chemical species concentration and chemical reaction products during discharge in a discharge region. The discharge is started at $t = 0$ s, when pulsed high voltage is applied at E/N = 100 Td. The initial conditions are atmospheric pressure and a temperature of 300 K. The electrons are accelerated by applying a high electric field, and each species are produced by electron impact as shown by the chemical reactions of numbers 1, 2, 5 and 6 in Table 1. The species balance is achieved about 0.1 ms after application of the electric field. During a discharge, the number of O radicals is the largest at $2 \times 10^{25}/m^3$ and that of N radicals is second largest. The number of electrons is the same as that of NO^+. A small amount of NO is produced.

Fig. 13 shows the decay process of the chemical species concentration and chemical reaction products after the discharge is turned off at $t = 0$ s. The initial condition results from species balance as obtained in Fig. 12. O, N, NO^+ and e begin to decrease at 0.01 ms. On the other hand, O_2 and NO increase due to recombination as detected by mass spectrometry in Fig. 7. N_2^+ decreases rapidly in all chemical species. Although the exact comparison can not be made with the available literature [20] due to the smaller value of E/N under the different discharge mode in the present study, the concentration of produced O radical in this study is one order higher at most and O radical decays more gradually after the discharge compared with the literature [20].

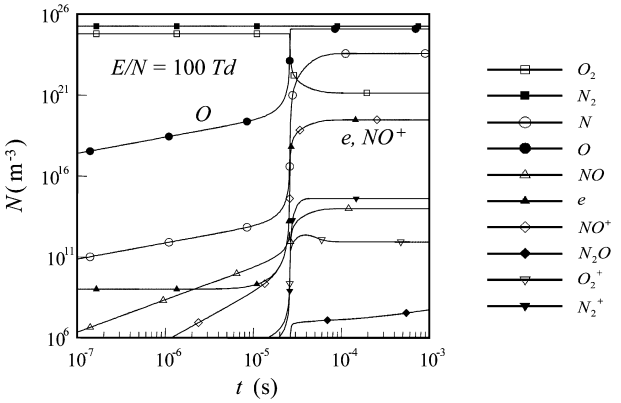

Fig. 12. Time evolution of chemical species concentration and chemical reaction products during discharge.

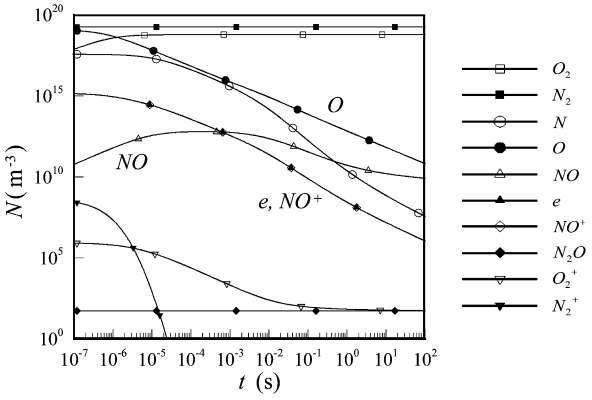

Fig. 13. Decay process of the chemical species concentration and chemical reaction products after discharge is turned off.

5. Conclusions

Experimental and numerical analyses were conducted to clarify the thermofluid field, and the chemical species of air plasma flow by pulsed arc discharge with small power for lean combustion enhancement and surface treatment. The results obtained in the present study are as follows.

(1) O, N radicals and NO can be produced in an air plasma flow by pulsed arc discharge, even with small input power. Downstream gas temperature and O radicals increase with the duty ratio at high surrounding pressure. However, there is a small effect of pulsed frequency on the gas temperature.
(2) It was numerically shown that the jet elongates continuously downstream but that a thermal vortex is generated at the torch exit at every pulsed discharge. It is diffused radially and is convected downstream. There is a good agreement of the time-averaged gas temperature and the measured bulk temperature at the centerline.
(3) The time evolution of production and the decay processes of the chemical species in the pulsed discharge region were clarified numerically using a simplified chemical reaction model. O and N radicals were considerably produced in the equilibrium state about 0.1 ms after the pulsed discharge. O and N radicals decreased but NO increased as a second product 0.01 ms after the pulsed discharge was turned off.

Acknowledgements

The present work was partly supported by a Grant-in-Aid for Scientific Research (A) from the Japan Society for the Promotion of Science. We sincerely thank Associate Professor T. Sato of our institute for his valuable advice.

References

[1] Japan Society of Mechanical Engineers, Functional Fluids and Intelligent Fluids, Corona Publishing Co. Ltd., Tokyo, 2000, pp. 48–92 (in Japanese).
[2] B.N. Ganguly, Plasma assisted improvement of high speed high altitude aerospace vehicle design, in: Proceedings of the XV International Conference on Gas Discharges and their Applications, Toulouse, 2004, pp. 1017–1023.
[3] A. Klimov, V. Bityurin, I. Moralev, B. Tolkunov, V. Vystavkin, Plasma assisted combustion of non-premixed hydrocarbon fuel in high-speed airflow, in: Proceedings of the 17th International Symposium on Plasma Chemistry, 2005, CD-ROM.
[4] K. Takita, N. Abe, G. Masuya, Y. Ju, Ignition enhancement by additional of NO and NO_2 from a N_2/O_2 plasma torch in a supersonic flow, Proc. Combust. Inst. 31 (2) (2007) 2489–2496.
[5] I.M. Vince, F.J. Weinberg, Hydrogen atom distribution in pulsed plasma jet igniters, Combust. Flame 67 (3) (1987) 259–264.
[6] E. Murase, S. Ono, K. Hanada, S. Nakahara, H. Endo, A.K. Oppenheim, Combustion enhancement of lean mixture by plasma jet ignition and pulsed jet ignition, Trans. Jpn. Soc. Mech. Eng. Ser. B 58 (546) (1992) 561–567.
[7] J.F. Behnke, H. Steffen, A. Sonnenfeld, R. Foest, V. Lebedev, R. Hippler, Surface modification of aluminium by dielectric barrier discharges under atmospheric pressure, in: A. Haljaste, T. Plank (Eds.), Proceedings of the 8th International Symposium on High Pressure Low Temperature Plasma Chemistry (HAKONE 8), Tartu, Estonia, vol. 2, 2002, pp. 410–414.
[8] R. Thyen, K. Höpfner, N. Kläke, C.-P. Klages, Cleaning of silicon and steel surfaces using dielectric barrier discharges, Plasmas Polym. 5 (2) (2000) 91–102.
[9] S.A. Bozhenkov, S.M. Starikovskaia, A.Y. Starikovskii, Nanosecond gas discharge ignition of H_2– and CH_4– containing mixtures, Combust. Flame 133 (1–2) (2003) 133–146.

[10] I.M. Vince, C. Vovelle, F.J. Weinberg, The effect of plasma jet ignition on flame propagation and sooting at the rich limit of flammability, Combust. Flame 56 (1) (1984) 105–112.
[11] A.Y. Starikovskii, Plasma supported combustion, Proc. Combust. Inst. 30 (2) (2005) 2405–2417.
[12] NIST Atomic Spectra Database, http://www.physics.nist.gov/cgi-bin/AtData/main_asd.
[13] I. Nakamori, T. Ikohagi, Numerical investigation of compressibility effect on turbulent covette flow using large-eddy simulation, Comput. Fluid Dyn. J. 8 (2) (1999) 243–249.
[14] Y. Tanaka, K.C. Paul, T. Sakuta, Thermodynamic and transport properties of N_2/O_2 mixtures at different admixture ratios, Trans. Inst. Electrical Eng. Jpn. 120-B (1) (2000) 24–30.
[15] I.A. Kossiy, A.Y. Kostinsky, A.A. Matveyev, V.P. Silakov, Kinetic scheme of the non-equilibrium discharge in nitrogen–oxygen mixtures, Plasma Sources Sci. Technol. 1 (3) (1992) 207–220.
[16] S.O. Macheret, M.N. Shneider, Modeling of air plasma generation by repetitive high-voltage nanosecond pulses, IEEE Trans. Plasma Sci. 30 (3) (2002) 1301–1314.
[17] G.V. Nadis, Modelling of plasma chemical processes in pulsed corona discharges, J. Phys. D: Appl. Phys. 30 (8) (1997) 1214–1218.
[18] M.S. Benilov, G.V. Naidis, Modelling of low-current discharges in atmospheric-pressure air taking account of non-equilibrium effects, J. Phys. D: Appl. Phys. 36 (15) (2003) 1834–1841.
[19] H. Kusunoki, K. Ito, K. Onda, Numerical analysis of repetitive pulsed-discharge DeNO process with ammonia injection, Inst. Electrical Eng. Jpn., Trans. Power Energy 123 (12) (2003) 1546–1553.
[20] K. Ito, K. Hagiwara, H. Nakaura, K. Onda, H. Tanaka, Numerical analysis of effects of electric field and pulse duration on discharge DeNOx performance, Trans. Inst. Electrical Eng. Jpn. 120-A (11) (2000) 979–986 (in Japanese).